Fabrication of Graphene–Quantum Dots Composites for Sensitive Electrogenerated Chemiluminescence Immunosensing

*Ling-Ling Li, Kun-Ping Liu, Guo-Hai Yang, Chun-Ming Wang, Jian-Rong Zhang, and Jun-Jie Zhu**

A novel strategy is reported for the fabrication of poly(diallyldimethylammonium chloride) (PDDA)-protected graphene–CdSe (P-GR-CdSe) composites. An advanced electrogenerated chemiluminescence (ECL) immunosensor is proposed for the sensitive detection of human IgG (HIgG) by using the as-prepared P-GR-CdSe composites. The P-GR-CdSe composite film shows high ECL intensity, good electronic conductivity, fast response, and satisfactory stability, all of which holds great promise for the fabrication of ECL biosensors with improved sensitivity. After two successive steps of amplification via the conjugation of PDDA and gold nanoparticles (GNPs) in the film, high ECL intensity is observed. The ECL immunosensor has an extremely sensitive response to HIgG in a linear range of 0.02–2000 pg mL^{-1} with a detection limit of 0.005 pg mL^{-1}. The proposed sensor exhibits high specificity, good reproducibility, and long-term stability, and may become a promising technique for protein detection.

1. Introduction

Since its discovery by K. S. Novoselov and A. K. Geim in 2004,[1] graphene, a single layer of carbon atoms densely packed in a honeycomb two-dimensional (2D) lattice,[2] has become a rapidly rising star among carbon materials, triggering a gold rush to exploit its possible applications in both experimental and theoretical studies. Graphene is considered a basic building block for graphitic materials of all other dimensionalities, and can be converted into fullerenes, carbon nanotubes, or 3D graphite via wrapping, rolling, or stacking, respectively.[3] It has been demonstrated that graphene has unique electronic, thermal, and mechanical properties,[4] such as massless Dirac fermions,[5] the quantum Hall effect,[6] ambipolar electric field effect,[1] superior thermal conductivity, and mechanical stiffness.[7] These characteristics drive the dreams of applying graphene in various areas, such as microelectrical devices, liquid-crystal devices, solar cells, sensitive sensors, and composite materials.[7–11] As for many other nanomaterials, a central challenge in the practical application of graphene is the prevention of aggregation, which is of particular importance for graphene sheets because most of the unique properties are only associated with individual sheets.[2,4] This obstacle could be overcome through covalent modification or noncovalent functionalization,[12] and the latter is particularly attractive since it can be combined with chemical handling through van der Waals forces or π–π interactions without destroying the electronic π system.[2] Some kinds of aromatic molecules and polymers were reported to noncovalently functionalize graphene,[2,7,13] which could provide an opportunity not only to improve the solubility and self-assembly properties of graphene,[13] but also to tailor their electronic properties in a desired manner.[2] In addition, different varieties of nanoparticles, such as Pd,[14] Pt,[14,15] Au,[16] and TiO_2,[17] were reported to decorate graphene sheets, which provides a new way to develop catalytic, magnetic, and optoelectronic materials. Semiconductor nanocrystals, known as quantum dots (QDs), were also selected for the synthesis of graphene–QD composites from graphene oxide (GO) by a one-step reaction[18,19] or via π–π stacking between graphene and QDs.[20] However, the composites synthesized through in situ reduction of GO produce QDs with relatively large dimensions,[18,19] which might limit their applications in optics. As the reports involving graphene–QD composites mainly focused on their optoelectronic behavior,[18,20] it is promising to study their properties and applications in other fields, such as biosensors.

Electrogenerated chemiluminescence (ECL) is light emission that arises from the high-energy electron-transfer reaction between electrogenerated species,[21] and which has many advantages over photoluminescence techniques, such as low cost, wide range of analytes, and high sensitivity.[22] Since Ding and Bard reported the ECL of Si QDs in 2002,[23] QDs have been widely used for constructing ECL sensors.[24–26] To improve the ECL intensity and biocompatibility, QD-based composites, especially carbon nanotubes (CNT)–QD composites,[26,27] have received particular interest due to their remarkable nanostructure, fast electron transfer, and excellent electrocatalytic activity of CNTs.[15,26]

L.-L. Li, K.-P. Liu, G.-H. Yang, Prof. J.-R. Zhang, J.-J. Zhu
Key Lab of Analytical Chemistry for Life Science (MOE)
School of Chemistry and Chemical Engineering
Nanjing University
Nanjing, 210093, P. R. China
E-mail: jjzhu@nju.edu.cn
K.-P. Liu, Prof. C.-M. Wang
School of Chemistry and Chemical Engineering
Lanzhou University
Lanzhou, 730000, P. R. China

DOI: 10.1002/adfm.201001550

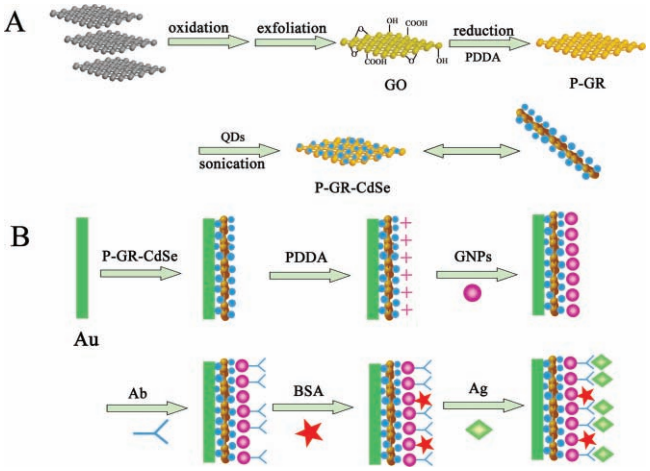

Scheme 1. A) Schematic representation of preparation procedure of P-GR-CdSe composites, including the oxidation of graphite (gray blocks) to graphite oxide (GO) with abundant oxygen functionalities, the in situ reduction of GO in the presence of PDDA to obtain positively charged PDDA protected graphene (P-GR) colloids, and the preparation of P-GR-CdSe composites via electrostatic interactions under sonication. B) Schematic illustration of the stepwise immunosensor fabrication process, including the formation of P-GR-CdSe composite film on the Au electrode, the linkage of PDDA to the film, the conjugation of GNPs to PDDA, the immobilization of antibody (Ab) on the electrode via GNPs, and the specific immunoreaction.

Although graphene sheets have higher conductivity, larger specific surface area, and lower manufacturing costs than CNTs,[7,28,29] reports concerning the ECL of graphene derivatives are relatively scarce.[21,30,31] ECL of partially oxidized highly oriented pyrolytic graphite surfaces and graphene oxide nanoparticles was reported,[30] and graphene oxide amplified ECL in the presence of QDs for the determination of glutathione from thiol-containing compounds was studied.[21] However, graphene oxide is electrically insulating and is conceptually different from graphene,[7,32] which may limits its applications. Therefore graphene is promising for constructing novel ECL biosensors.

Herein, as shown in **Scheme 1**, we present a novel strategy for the preparation of graphene-QD composites via electrostatic interactions between negatively charged thioglycolic acid (TGA) modified CdSe QDs and positively charged graphene, which was noncovalently functionalized with poly (diallyldimethylammonium chloride) (PDDA) via an exfoliation/in situ reduction of GO in the presence of PDDA. An advanced label-free ECL immunosensor is proposed for the first time by using the as-prepared composites (P-GR-CdSe composites) from a layer-by-layer assembly process. The interfusion of PDDA-protected graphene (P-GR) with CdSe QDs film not only improved the ECL intensity, response speed, and stability, but also provided a large specific surface for high levels of protein loading, which resulted in extreme sensitivity. Positively charged PDDA was electrostaticly adsorbed to the composite film, which also acted as the binding linker for negatively charged gold nanoparticles (GNPs). The conjugation of PDDA and GNPs enhanced the ECL intensity. Then antibody (Ab), goat anti–human IgG, was linked to the P-GR-CdSe/PDDA/GNP film. After blocking with bovine serum albumin (BSA), the electrode could be used as an ECL immunosensor for the detection of human IgG (HIgG, denoted Ag). This research expands graphene applications and also provides a versatile avenue for ECL study. Scheme 1 outlines the fabrication procedures for the P-GR-CdSe composites (A) and the ECL immunosensor (B).

2. Results and Discussion

2.1. Characterization of GR and P-GR

As described previously,[33,34] the mechanism of GO preparation mainly involves the generation of oxygen-containing groups and the conversion of sp^2 bonds into sp^3 bonds. The graphene sheets in GO are heavily oxygenated, as they are decorated mostly with epoxide and hydroxyl groups on their basal planes,[7,35] in addition to carbonyl and carboxyl groups located at the sheet edges, as shown in Scheme 1A. This oxygenation may weaken the van der Waals interactions between the layers of GO and make them strongly hydrophilic, which thus facilitates their hydration and exfoliation in aqueous media. On the other hand, the reduction process is mainly the removal of oxygen functionalities with partial restoration of aromatic graphene network (sp^2),[35,36] which results in hydrophobic GR sheets, so agglomerate and eventually precipitate could be obtained even under ultrasonication. After GR sheets were modified with positively charged PDDA, the obtained sheets were hydrophilic and soluble in the presence of a static repulsion force. The polyelectrolyte PDDA acted as a primer on the GR surface for the subsequent homogeneous adsorption of CdSe QDs through electrostatic interactions.

The oxygen functionalities on the GO surface and the deoxygenation on the GR surface, as well as the existence of PDDA, were confirmed by using Fourier-transform infrared spectroscopy (FTIR). **Figure 1**A shows the typical FTIR spectrum obtained for the three graphene substrates (GO, GR, and P-GR). The spectrum of GO illustrates the presence of C–O (ν_{C-O} at 1110 cm^{-1}), C–OH (ν_{C-OH} at 1395 cm^{-1}), C=O ($\nu_{C=O}$ at 1733 cm^{-1} in carboxylic acid and carbonyl moieties),[16,37,38] and

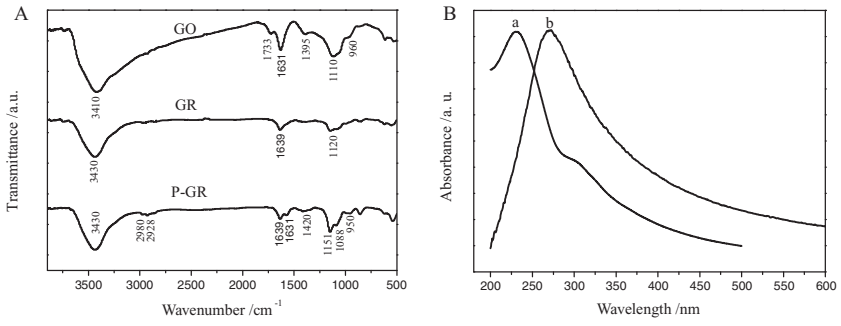

Figure 1. A) FTIR spectra of GO, GR, and P-GRB) UV–vis absorption spectrum of GO (a) and P-GR (b).

C–O–C stretches (ν_{C-O-C} at 960 cm^{-1}).[39] The peak at 1631 cm^{-1} can be attributed to the stretching deformation vibration of intercalated water and the skeletal vibrations of unoxidized graphitic domains.[13,40] The spectrum also shows a broad, intense band at 3410 cm^{-1} that corresponds to O–H stretching vibrations of the O–H groups originating from carboxylic acid as well as intercalated water.[40] Compared with GO, the spectrum of GR is essentially featureless except the C=C peak at 1639 cm^{-1}, and a sharper O–H peak at 3430 cm^{-1}. There is also a residual C–O band at 1120 cm^{-1}, whereas other adsorption bands of oxygen functionalities mostly disappeared (C=O, epoxy groups etc), which suggests considerable deoxygenation by the chemical reduction process. In the case of P-GR, the spectrum shows the characteristic absorption bands of PDDA, such as the C–H asymmetric and symmetric stretching frequencies (2980 and 2928 cm^{-1}, respectively), CH_2 bending vibrations (1420, and 950 cm^{-1}), and C–N symmetric stretching vibration (1088 cm^{-1}),[41] which reflect the presence of PDDA.

Figure 1B shows the UV-vis absorption spectra of P-GR and GO dispersions for comparison. In the spectrum of GO, there are two absorption features: a peak at 230 nm due to the $\pi \rightarrow \pi^*$ transition of C=C, and a shoulder at about 300 nm corresponding to the $n \rightarrow \pi^*$ transition of the C=O bond.[42] For P-GR, the absorption peak corresponding to the $\pi \rightarrow \pi^*$ transition red-shifts to 270 nm, which is consistent with the absorption of aqueous stable graphene sheets, suggesting that the electronic conjugation within the graphene sheets is restored after the reduction.[4]

The surface charge of the as-prepared P-GR was determined to be +55 mV by zeta potential. This potential is ideal for stabilizing a conventional aqueous dispersion, as the American Society for Testing and Materials (ASTM) defines colloids with zeta potentials higher than 40 mV (negative or positive) as having good stability.[38]

2.2. Characterization of P-GR-CdSe Composites

High-resolution transmission electron microscopy (HRTEM) images were taken to observe the morphology of G-PR and P-GR-CdSe composites. **Figure 2**A shows the HRTEM image

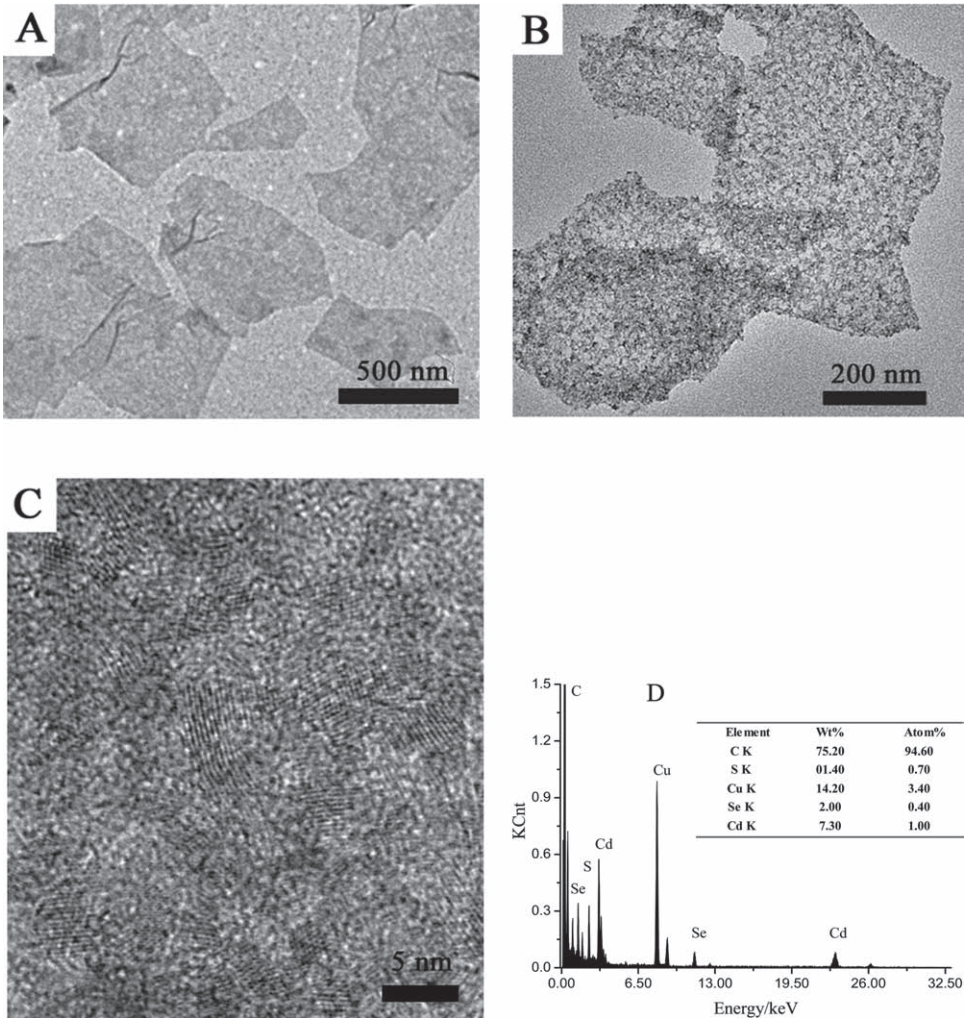

Figure 2. HRTEM images of A) P-GR, B) P-GR-CdSe composites, and C) the magnified image of CdSe crystals on a P-GR sheet. D) The SAEDX analysis of P-GR-CdSe composites shown in panel B.

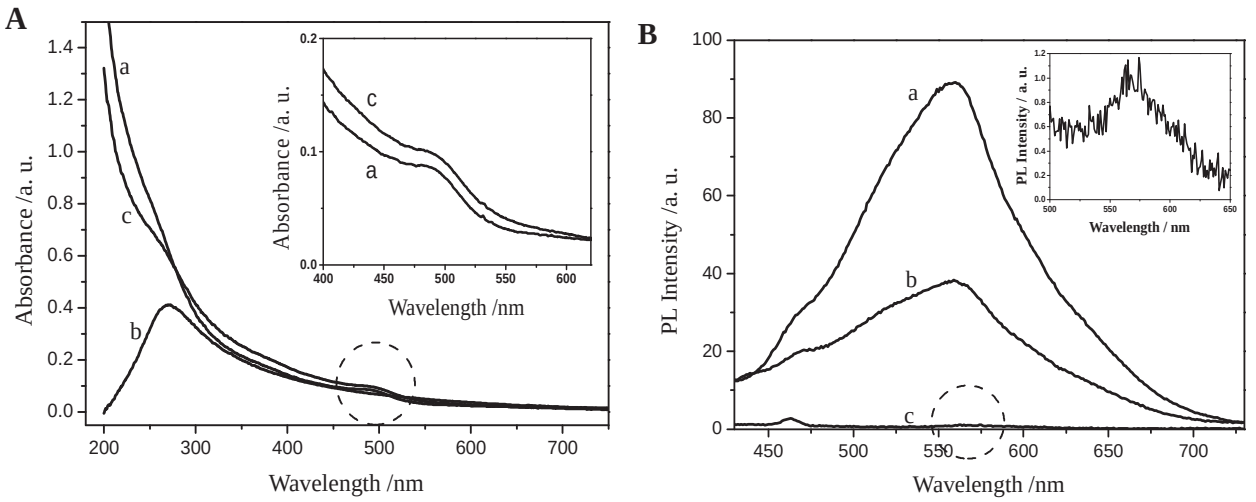

Figure 3. A) UV–vis absorption spectrum of a) free CdSe QDs, b) P-GR, and c) P-GR-CdSe composites. Inset: Amplification of the absorption spectrum of free CdSe QDs and P-GR-CdSe composites. B) Photoluminescence of a) free CdSe QDs, b) P-GR-CdSe composites, and c) the supernatant after centrifugation of the P-GR-CdSe composites. Inset: Amplification of curve c between 500–650 nm. Excitation wavelength: 400 nm.

of P-GR sheets with corrugated flakelike shapes. Mono-layer sheets could be observed in most of regions, whereas restacked parts and wrinkles could also be seen, which could be attributed to electronic repulsion between the soft and flexible layers. Figure 2B shows a representative HRTEM image of the P-GR-CdSe composites. The homogeneous and dense coverage of QDs on the graphene surface could be observed. No aggregation of P-GR sheets or free QDs was observed, which suggests complete deposition of the CdSe QDs. Moreover, the electrostatic forces were strong enough for the attachment of CdSe QDs to P-GR, which was confirmed by the absence of luminescence from the supernatant after centrifugation of the P-GR-CdSe composites (curve c, **Figure 3**B). The lattice image of QDs is shown in Figure 2C, from which the crystalline features of CdSe QDs can be clearly observed. Furthermore, the QDs were reasonably monodisperse, with an average size of about 2.5 nm. The composition of P-GR-CdSe composites was further confirmed by means of selected area energy dispersive X-ray analysis (SAEDX), as shown in Figure 2D. The result revealed the composition was mainly C, Cu, S, Se, and Cd. Strong signals from Cd, Se, and S suggested the identity of the QDs coupled onto the P-GR sheets. The Cu and C peaks observed in the spectrum could be attributed to the Cu grid and graphene substrate. Moreover, the molar ratio of Se to Cd and S was calculated to be 0.91, approximate to the theoretical value of 1.[43]

The absorption and room-temperature photoluminescence (PL) spectra of CdSe QDs are displayed in Figure 3. The PL emission peak at 560 nm and absorption maximum at 480 nm indicate the consequence of quantum confinement.[44,45] Estimated from the first excitonic adsorption peak in the UV–vis spectrum by several empirical equations,[46] the size of QD particles and molar concentration of QD solution were 2.1 nm and 212 μM, respectively (Supporting Information). The calculated size of QDs was consistent with HRTEM observations.

For comparison, the absorption spectra of P-GR before and after deposition of the CdSe QDs were also plotted (Figure 3A). Previous investigations reported that no QD absorption band could be observed after QDs were attached to CNTs because the broad background absorption of the CNT could strongly screen the absorption of the QDs; only if QDs were densely coated on to the CNT could the absorption band be seen.[47] However, the first excitonic adsorption peak of CdSe in our experiment could still be observed (inset in Figure 3A), which suggests a dense coating of QDs on the P-GR sheets. Moreover, no obvious change of the absorption peak of the QDs was observed, which indicates that almost no QD agglomerate was formed on the P-GR sheets,[48] consistent with HRTEM observations.

The PL emission spectrum of P-GR-CdSe composites (Figure 3B) shows a dramatic decrease in intensity compared with that of pure QDs, which indicates partial quenching. This result can be ascribed to the electron transfer from excited CdSe QDs to graphene.[18] Similar PL quenching was observed in previous reports on CNT–QD composites.[47–49] Furthermore, the almost constant size distribution of CdSe QDs was verified again by the neglectable red shift (1 nm) of the QD band-gap emission after adsorption onto the GR sheets.[19]

2.3. Electrochemical and ECL Behaviors of the P-GR-CdSe Composites

Prior to ECL investigation, we first studied the electrochemical behavior of P-GR. **Figure 4**A depicts the cyclic voltammograms (CV) of $[Fe(CN)_6]^{3-/4-}$ at bare Au electrode, PDDA-protected MWCNTs modified Au electrode (P-CNT/Au electrode), and P-GR/Au electrode. According to Randles–Sevcik equation:[50]

$$i_p = 2.69 \times 10^5 n^{3/2} A D^{1/2} V^{1/2} C_0$$

where i_p is the peak current, n is the number of electrons for the reaction, A is the apparent electrode area [cm^2], D is the diffusion coefficient of the redox probe [cm^2 s^{-1}], v is CV scanning rate [V s^{-1}], and C_o is the bulk concentration of

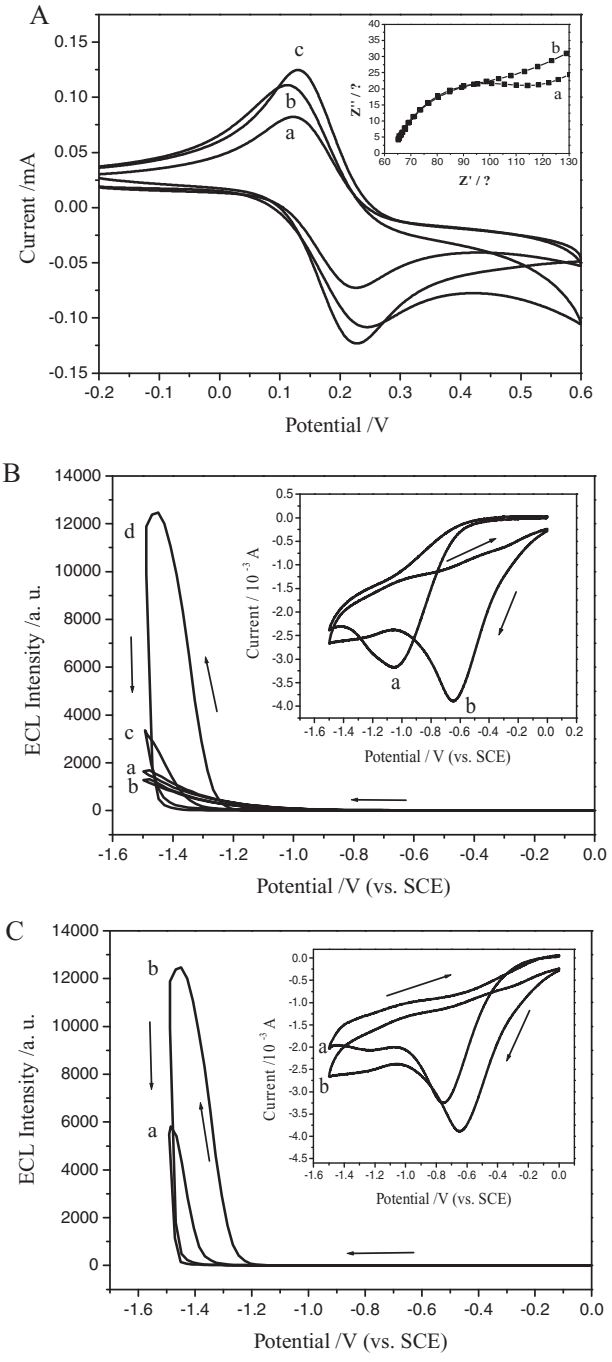

Figure 4. A) Cyclic voltammograms (CVs) of a) bare Au electrode, b) P-CNT/Au electrode and c) P-GR/Au electrode recorded in 10 mM PBS (2.5 mM $[Fe(CN)_6]^{3-/4-}$ + 0.1 M KCl, pH 7.4). Inset: EIS of a) P-CNT/Au electrode and b) P-GR/Au electrode in 10 mM PBS (2.5 mM $[Fe(CN)_6]^{3-/4-}$ + 0.1 M KCl, pH 7.4). The frequency range was 0.01–100000 Hz with a signal amplitude of 5 mV. Scan rate: 100 mV s^{-1}. B) ECL–potential curves of a) bare Au electrode, b) P-GR/Au electrode, c) free CdSe QDs/Au electrode, and d) P-GR-CdSe/Au electrode in 0.1 M PBS (pH 7.4) containing 0.1 M $K_2S_2O_8$ and 0.1 M KCl. Inset: CVs of a) free CdSe QDs/Au electrode and b) P-GR-CdSe/Au electrode. C) ECL–potential curves and CVs (inset) of a) P-CNT-CdSe/Au electrode and b) P-GR-CdSe/Au electrode. Scan rate: 200 mV s^{-1}. The voltage of the photomultiplier tube (PMT) was set at 800 V for the bare and P-GR modified electrodes and 600 V for the other electrodes.

$[Fe(CN)_6]^{3-/4-}$ [mol cm^{-3}]. Herein, $n = 1$ and D is assigned as 1×10^{-5} cm^2 s^{-1}. Thus the sequence of the calculated values of A for the electrodes is P-GR/Au electrode (curve c, 0.195 cm^2) > P-CNT/Au electrode (curve b, 0.168 cm^2) > Au electrode (curve a, 0.125 cm^2). The largest value of A was obtained at the P-GR/Au electrode, which indicates this has many more binding sites for QDs than the other two electrodes, and subsequently protein. Furthermore, the extraordinary electron transport properties and high conductivity of P-GR could be observed using electrochemical impedance spectroscopy (EIS; inset in Figure 4A).

The ECL intensity of the P-GR film (Figure 4B) showed only a slight decrease compared with that of the bare electrode due to the nonconductive property of PDDA,[51] which further indicates the high conductivity of the graphene-based composite film.

Additionally, to investigate the effect of P-GR on the electrochemical and ECL behaviors, free CdSe QD modified Au electrode was prepared, containing the same quantity of QDs as the P-GR-CdSe modified electrode. Prior to use, the two modified electrodes were transferred to pH 7.4 phosphate-buffered saline (PBS) for 15 min to remove unabsorbed materials. As shown in Figure 4B, curves c and d depict the ECL-potential curves of the pure CdSe QD and P-GR-CdSe composite films, respectively. One peak could be observed in both curves, resulting from the reaction between CdSe QDs and $S_2O_8^{2-}$. Obviously, the ECL intensity was much higher than that of pure CdSe QD film. It is worth noting that the ECL curve of the composite film showed emission peak at −1.45 V, with an onset potential at about −1.20 V that was much more positive than that of pure CdSe QD film. The result indicates that the presence of P-GR decreased the potential barriers of the ECL reduction, which could be attributed to the extraordinary electron transport of graphene. Furthermore, due to the large specific surface area of graphene, as confirmed above, P-GR sheets may partly act as an effective platform, providing more binding sites for the adsorption of CdSe QDs, whereas the bare Au electrode can only adsorb a few QDs due to the electrostatic repulsion of negatively charged QDs. On the other hand, a larger specific surface area in the composite film could also facilitate the diffusion of $K_2S_2O_8$ into the membrane, resulting in the occurrence of ECL signal not only at the interface but also in the nanocrystalline film.[26] The ECL signal of P-GR-CdSe modified electrode could reach the maximum value and maintained balance only for 3 min, whereas the free CdSe QD modified electrode took more than 15 min, which indicates a fast response of the composite film. The CVs of the two films were also recorded simultaneously (inset in Figure 4B). One cathodic peak appeared in both CVs which corresponding to the reduction of $S_2O_8^{2-}$.[26,45] The more positive reduction potential and higher reduction current suggested that P-GR could accelerate electron transfer between the electrode and species in solution, i.e. $S_2O_8^{2-}$.

Moreover, PDDA-protected MWCNTs-CdSe composites (P-CNT-CdSe) with the same concentration as the P-GR-CdSe were also prepared for parallel experiments. Both the electrochemical and ECL behaviors of the two composite-modified Au electrodes were studied (Figure 4C). The P-GR-CdSe composite film exhibited higher ECL intensity, more positive ECL onset potential and peak position, as well as more positive reduction potential and higher

reduction current (inset in Figure 4C) than those of the P-CNT-CdSe film. Thus graphene can be an excellent inexpensive candidate for electrochemical investigation and construction of sensors.

2.4. Fabrication and Characterization of the ECL Immunosensor

As shown in Scheme 1, for the preparation of the ECL immunosensor, P-GR-CdSe composites were firstly coated onto the electrode, which bore negative charges on the surface, and then PDDA with positive charge was electrostaticly absorbed to the composite film, which also acted as the binding linker for negatively charged GNPs. The isoelectric point (pI) of IgG is close to 7.0, and therefore, in pH 6.0 PBS, Ab should bear a net positive charge.[51] When the P-GR-CdSe/PDDA/GNP modified electrode was dipped into the Ab solution, Ab could be firmly attached onto the electrode through electrostatic interactions and interaction between the GNPs and mercapto or primary amine groups of Ab.

ECL signals at each immobilization steps were recorded to monitor the fabrication of the immunosensor (**Figure 5**A). After PDDA was conjugated onto the P-GR-CdSe composite film (Figure 5A, curve a), the resulting electrode showed a great enhancement in ECL intensity (Figure 5A, curve b) which was ascribed to the effect of the amine groups of PDDA.[45] Hence the PDDA decorated on the GR sheets might also contribute to the high ECL intensity, which conjugated to the CdSe QDs in a reverse-sandwich-like manner together with the latter PDDA layer. By the assembly of GNPs onto the P-GR-CdSe/PDDA modified electrode surface (Figure 5A, curve c), the ECL signal was further amplified. The adsorbed conductive GNPs may act as a conductive wire to facilitate the electron transfer in the ECL reaction. It is noteworthy that the voltage of the PMT upon the modification of GNPs was specially set at 400 V because of the high reading of 17700 counts on the maximum scale of the ECL analyzer. Then the following modification steps (Figure 5A, curve d, e, and f), i.e. the conjugation of Ab, BSA, and HIgG, resulted in the gradual decrease in ECL intensity originating from the inert protein layers, which generated a barrier for electron and mass transfer and significantly slowed down the diffusion rate of ECL reagents towards the electrode surface, leading to the decrease of ECL signal.

Electrochemical impedance spectroscopy is an effective method for monitoring the changes in the surface features of the modified electrodes in the assembly process.[52,53] The impedance spectra include a semicircle portion and a linear portion. The semicircle portion at higher frequencies corresponds to the electron-transfer-limited process, and the linear portion at lower frequencies represents the diffusion-limited process. The semicircle diameter equals the electron-transfer resistance, R_{et}.[54] Figure 5B shows the Nyquist plots of EIS observed upon the stepwise modification processes in 10 mM PBS (2.5 mM $[Fe(CN)_6]^{3-/4-}$ + 0.1 M KCl, pH 7.4). The bare Au electrode revealed a small semicircle domain (Figure 5B, curve a), which implies a low R_{et} value of the redox couple, i.e. $[Fe(CN)_6]^{3-/4-}$. All modified electrodes showed a large increase in diameter over that of the bare Au electrode, which indicates much higher R_{et} values after modification. Due to its nonconductive properties,[51] PDDA could inhibit the electron transfer, leading to increased resistance for the redox probe. After modification with GNPs, the resulting electrode showed a much lower resistance, which implies that the conductive GNPs accelerated the electron transfer. It has been reported that the antigen–antibody complex could act as a layer disturbing ion diffusion and changing electrical capacitance, and both factors would significantly affect the electrochemical impedance of electrodes during the formation of antigen–antibody complex.[53] This suggestion is consistent with the observed greatly increased R_{et} value via the anchor of Ab, BSA, and HIgG (Figure 5B, curve

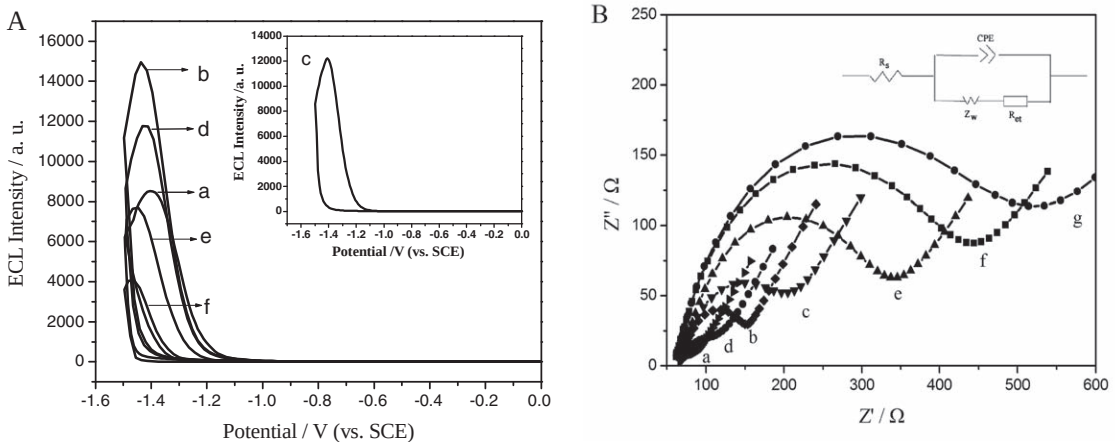

Figure 5. A) ECL–potential curves of a) P-GR-CdSe, b) P-GR-CdSe/PDDA, c) P-GR-CdSe/PDDA/GNPs, d) P-GR-CdSe/PDDA/GNPs/Ab, e) P-GR-CdSe/PDDA/GNPs/Ab/BSA, and f) P-GR-CdSe/PDDA/GNPs/Ab/BSA/HIgG modified Au electrodes, scanning from 0 V to −1.5 V with a scan rate of 200 mV s^{-1}. The voltage of the PMT was set at 500 V (inset 400 V). B) EIS of a) bare electrode, b) P-GR-CdSe, c) P-GR-CdSe/PDDA, d) P-GR-CdSe/PDDA/GNPs, e) P-GR-CdSe/PDDA/GNPs/Ab, f) P-GR-CdSe/PDDA/GNPs/Ab/BSA, and g) P-GR-CdSe/PDDA/GNPs/Ab/BSA/HIgG modified Au electrodes in 10 mM PBS (2.5 mM [Fe (CN) 6]$^{3-/4-}$ + 0.1 M KCl, pH 7.4). The frequency range was 0.01–100000 Hz with a signal amplitude of 5 mV. The inset shows the equivalent circuit to fit with obtained EIS spectra, where: RS is the uncompensated resistance, Z_w isthe finite-length Warburg element, CPE is the constant phase element attributed to the capacity of the double electric layer, and Ret is electron-transfer resistance attributed to the film modified on the electrode.

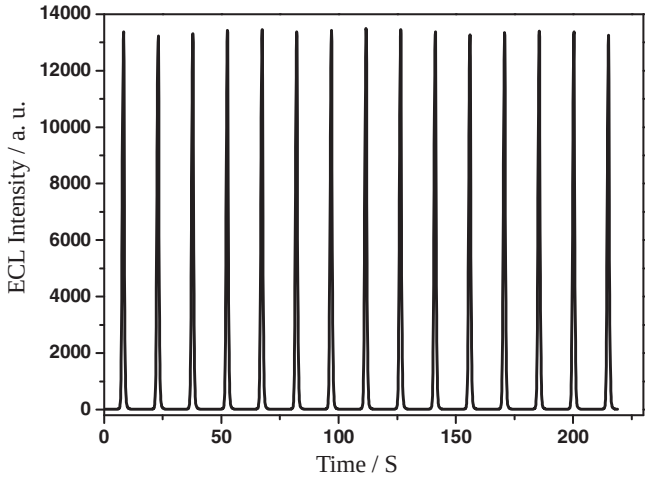

Figure 6. ECL emission of the immunosensor. Scan rate: 200 mV s^{-1}. The voltage of the PMT was set at 600 V.

e, f, g), and the same increment has also been reported in previous reports.[52–54]

In addition, equivalent circuit fitting with the obtained EIS spectra has also been depicted (inset in Figure 5B) according to previous reports.[53,54] Ideally, Z_w and R_s represent the bulk properties of the electrolyte solution and diffusion features of the redox probe in solution and, as demonstrated in Figure 5B, are not affected by modifications on the electrode surface,[54] whereas the changes in R_{et} value were much larger than those in other impedance elements. Thus, R_{et} was a suitable probe for monitoring the changes in the surface features of modified electrode in the assembly process.

2.5. Detection of HIgG

Figure 6 shows the ECL emission of the immunosensor after dipping in 0.2 pg mL^{-1} HIgG solution for 50 min under consecutive potential scans from 0 to –1.5 V for 15 cycles. The ECL signals were high and stable, which suggests that the sensor is suitable for ECL detection.

As confirmed above, when HIgG was immobilized on the electrode, the ECL intensity dramatically decreased due to the inert protein layer. The more HIgG that was immobilized, the weaker the ECL signal that could be obtained. **Figure 7**A shows the ECL responses of the immunosensor. As can be seen, the ECL peak intensity in the presence of HIgG was lower than that in the absence of HIgG, and decreased gradually with increasing concentrations of HIgG (b–g). Figure 7B illustrates a linear relationship of ECL intensity with the logarithm of HIgG concentration in a range from 0.02 to 2000 pg mL^{-1} (r = 0.997, n = 6, where r is the relative coefficient and n is the number of data points in the calibration curve). According to the linear equation, HIgG could be detected quantitatively. Higher serum HIgG levels could be detected by an appropriate dilution with pH 7.4 PBS. As can be observed, the decreases in ECL intensity were not obvious at higher HIgG concentrations beyond the detection range due to steric hindrance or saturation of coupled antigen.[52]

Due to the high conductivity of the graphene-based immunosensor and its high ECL intensity after two successive steps of amplification, small amounts of HIgG with poor conductivity on the electrode surface resulted in great changes in ECL response. Furthermore, the large specific surface area of graphene can afford a high protein loading. As a result, the sensor showed an extremely sensitive response to HIgG with a detection limit of 0.005 pg mL^{-1}.

2.6. Specificity, Reproducibility, and Stability of the Immunosensor

Specificity is an important criterion for immunosensors. The potential interference from coexisting species toward HIgG detection was studied by detecting the ECL response of the electrodes modified with the following two real samples: one containing 20 pg mL^{-1} HIgG, 50 pg mL^{-1} goat IgG, 50 pg mL^{-1} human alpha-fetal protein, and 100 pg mL^{-1} BSA, and the other composed of 20 pg mL^{-1} HIgG and 200 pg mL^{-1} goat IgG. No significant difference (R.S.D = 5.1% and 5.4%, respectively)

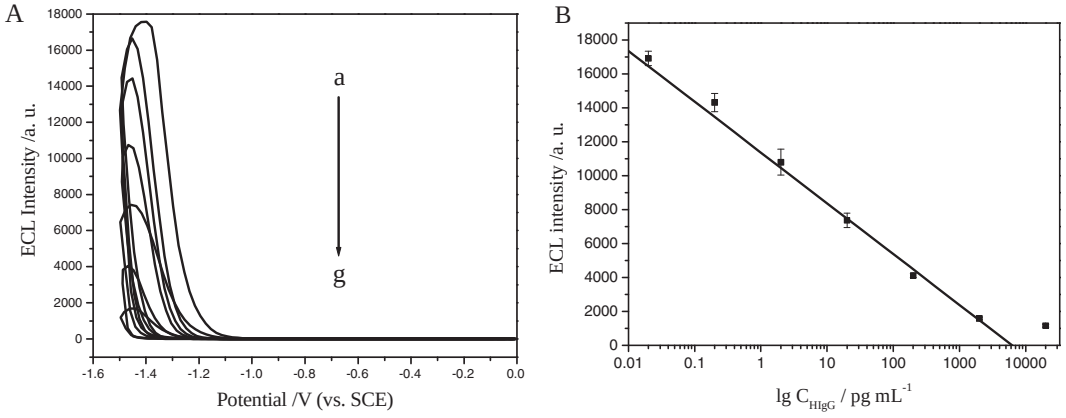

Figure 7. A) ECL–potential curves of the immunosensor in the absence (a) and presence (b–g) of different concentrations of HIgG (pg mL^{-1}): a) 0, b) 0.02, c) 0.2, d) 2, e) 20, f) 200, g) 2 000, scanning from 0 V to –1.5 V with a scan rate of 200 mV s^{-1}. The voltage of the PMT was set at 600 V. B) Calibration curve for HIgG determination. Error bars were calculated from triple parallel experiments.

Table 1. Comparison of serum HIgG levels determined using two methods.

Serum samples	1	2	3	4
Immunosensor [pg mL^{-1}][a)]	0.96	2.03	28.1	314.4
ELISA [pg mL^{-1}]	0.90	1.94	26.7	300.0
Relative deviation [%]	6.7	4.6	5.2	4.8

[a)] Average value from three successive determinations.

was observed from the result obtained in the presence of HIgG only. Thus, the immunosensor had a good specificity to HIgG, which makes this immunosensor feasible for the determination of IgG in human specimens.

The reproducibility of the immunosensor for HIgG was investigated with intra- and interassay precision, which were evaluated by measuring one HIgG level for three reduplicate measurements, and with three immunosensors made at the same electrode. The intra- and interassay variation coefficients obtained from 200 pg mL^{-1} HIgG were 3.2% and 8.5%, respectively, which indicate acceptable precision and fabrication reproducibility.

When the immunosensor was stored in pH 7.4 PBS at 4 °C for two weeks, no apparent change in the same HIgG concentration was found, which indicates that the immunosensor has good stability.

2.7. Application of the Immunosensor in Human IgG Levels

The feasibility of the immunoassay system for clinical applications was investigated by analyzing several clinical samples compared with the ELISA method performed in Nanjing Gulou Hospital. These serum samples were composed of IgG, IgA, IgM, complement component C3 and C4 etc., and detected with an appropriate dilution in pH 7.4 PBS. **Table 1** compares the two methods. The presented method is in acceptable agreement with the traditional ELISA method and thus may provide an alternative tool for detection of protein in clinical laboratories.

3. Conclusions

We have proposed a new strategy for the fabrication of an advanced ECL immunosensor by using PDDA-protected graphene. CdSe QDs were successfully attached to PDDA-protected graphene through electrostatic interactions, and the obtained P-GR-CdSe composites were used to construct an ECL immunosensor via layer-by-layer assembly. The as-prepared P-GR-CdSe composite film demonstrated excellent conductivity, extraordinary electron transport properties, and large specific surface area, which resulted in high ECL intensity and excellent film-forming ability and made it a promising candidate for development of an ECL immunosensor. The proposed immunosensor showed an extremely sensitive response to HIgG, which was validated by using the conventional ELISA method, with which it showed high consistency. Based on the parallel experiments with CNTs, graphene was confirmed as a promising inexpensive candidate. This research displays the powerful utility of graphene in ECL studies, and provides a convenient, low-cost, sensitive, and specific method for protein detection, which might provide an effective candidate in clinical laboratory.

4. Experimental Section

Chemicals and Materials: Multiwalled carbon nanotubes (MWCNTs, CVD method, purity >95%, diameter 30–60 nm, length 0.5–15 μm) were purchased from Nanoport. Co. Ltd. (Shenzhen, China). Graphite powder (KS-10, 99.95%) and PDDA (20%, w/w, in water, M_W = 200,000–350,000) were obtained from Sigma–Aldrich. Hydrazine hydrate (80%) was from Nanjing Chemical Reagents Factory (Nanjing, China). Chloroauric acid ($HAuCl_4$) and trisodium citrate were obtained from Shanghai Reagent Company (Shanghai, China). Gold nanoparticles were prepared by citrate reduction of $HAuCl_4$ in aqueous solution (Figure S1 and S2, Supporting Information).[44] Human IgG and goat anti–human IgG were purchased from Ningbo Xinzhi Biochemical Reagents (Ningbo, China). BSA (96–99%) was obtained from Sigma (St. Louis, MO, USA). Human alpha-fetal protein was purchased from Beijing Biosynthesis Biotechnology Co., LTD (Beijing, China). All other reagents were of analytical grade and used as received without further purification. 0.1 M PBS of various pH was prepared by mixing the stock solutions of NaH_2PO_4 and Na_2HPO_4, and then adjusting the pH with 0.1 M NaOH and H_3PO_4. 0.1 M PBS (pH 7.4) containing 0.1 M $K_2S_2O_8$ and 0.1 M KCl was used as the electrolyte in ECL analysis. Unless otherwise mentioned, ultrapure fresh water obtained from a Millipore water purification system (MilliQ, specific resistivity > 18MV cm^{-1}, S. A. Molsheim, France) was used throughout this work.

Apparatus: The ECL emission was detected with a Model MPI-A Electrochemiluminescence Analyzer (Xi'An Remax Electronic Science & Technology Co. Ltd., Xi'An, China) with a conventional three-electrode system composed of a platinum wire as the auxiliary electrode and a saturated calomel electrode (SCE) as the reference; working electrodes were bare or modified Au electrodes (4 mm diameter). The spectral width of the PMT was 200–800 nm and the PMT voltage was 400–800 V in the detection process. EIS was carried out on an Autolab PGSTAT12 (Eco chemie, BV, The Netherlands) and controlled by FRA 4.9 software, using the same three-electrode system as in the ECL detection. UV-vis spectra were recorded on a UV-3600 spectrophotometer (Shimadzu, Kyoto, Japan). PL spectra were obtained on a RF-5301PC spectrophotometer (Shimadzu, Kyoto, Japan). FTIR was measured on a Nicolet 6700 FTIR spectrometer (Nicolet, USA). HRTEM images were taken using a JEOL 2010 electron microscope at an accelerating voltage of 200 kV. Samples for HRTEM were prepared by placing two drops of the dispersed samples solution on a carbon-film-coated copper grid (400 mesh) and then drying under air.

Synthesis of Soluble P-GR and Pure Graphene: GO was synthesized from natural graphite powder by a modified Hummers and Offeman method as originally presented by Kovtyukhova et al. (Supporting Information).[37,55] P-GR was prepared according to our previous report.[56] First, 20% PDDA (0.5 mL) solution was added to 0.5% GO solution (100 mL) and stirred for 30 min. Then 80% hydrazine hydrate (0.5 mL) was added and stirring maintained for 24 h at 90 °C. Finally, the black P-GR could be obtained by filtration and washing with distilled water, and then redispersed readily in water upon mild sonication, forming a black suspension. The obtained P-GR dispersion (0.1 mg mL^{-1}) possessed good separation and stability due to electrostatic repulsion; there was no sign of coagulation of graphene sheets after more than six months. The preparation of pure graphene was similar to that of P-GR, except that no PDDA was added. PDDA-protected MWCNTs (P-CNT) with the same concentration as P-GR were also prepared for parallel experiments using a procedure reported previously.[57]

Preparation of P-GR-CdSe QDs Composites: Thioglycolic acid (TGA) modified CdSe QDs were prepared according to the literature.[26] To prepare P-GR-CdSe QDs composites, P-GR solution was mixed with CdSe QDs solution with the volume ratio of 1:1 under sonication for

30 min. The P-CNT-CdSe QDs composites were prepared by the same procedure.

Preparation of the ECL Immunosensor: An Au electrode was polished carefully with 1.0, 0.3, and 0.05 μm alumina powder on fine abrasive paper sequentially and then washed ultrasonically in water and ethanol for a few minutes. Prior to modification, the bare electrode was scanned in 0.5 M H_2SO_4 between –0.2 and 1.5 V until a reproducible CV was obtained. After the electrode was rinsed thoroughly with doubly distilled water and allowed to dry at room temperature, P-GR-CdSe QDs composite solution (10 μL) was dropped onto the electrode and dried in the air, followed by dropping 0.5% PDDA (10 μL) aqueous solution containing 0.5 M NaCl onto the electrode. After air-drying, the P-GR-CdSe/PDDA modified electrode was rinsed several times with water to remove the physically adsorbed PDDA. By preparing the electrode in this way, its surface was covered with positively charged PDDA that readily adsorbed GNPs with negative charge. After soaking in GNP solution for 8 h to obtain the P-GR-CdSe/PDDA/GNPs modified electrode, the electrode was rinsed with water and dipped in 0.5 mg mL^{-1} antibody solution (50 mM PBS, pH 6.0) at 4 °C overnight. Finally, it was rinsed with pH 7.4 PBS to remove physically adsorbed Ab and incubated in 50 μL of 2 wt% BSA at 37 °C for 1 h to block nonspecific binding sites. After rinsing with pH 7.4 PBS, the electrode was used as an ECL immunosensor, and incubated in 50 μL of HIgG samples at 37 °C for 50 min. The P-CNT-CdSe modified Au electrode was also fabricated by the same procedure. Moreover, P-GR and free CdSe QD modified electrodes were prepared containing equal quantities of P-GR or CdSe QDs to the as-prepared P-GR-CdSe modified electrode. All resulting electrodes were washed with water and stored at 4 °C when not in use.

The experimental parameters were all optimized by means of ECL experiments in 0.1 M PBS containing 0.1 M $K_2S_2O_8$ and 0.1 M KCl (Figure S3, S4 and S5, Supporting Information), which is similar to our previous method.[45]

ECL detection: The ECL immunosensors with different concentrations of HIgG were used in 0.1 M PBS (pH 7.4) containing 0.1 M $K_2S_2O_8$, and 0.1 M KCl, scanning from 0 V to –1.5 V with a scan rate of 200 mV s^{-1}.

Supporting Information

Supporting Information is available from the Wiley Online Library or from the author.

Acknowledgements

We greatly appreciate the support of the National Natural Science Foundation of China for the Key program (20635020), Creative Research Group (20821063), and General program (50972058). This work is also supported by the National Basic Research Program of China (2011CB933502). The authors thank Professor Kui Zhang from Nanjing Gulou Hospital for her kind help.

Received: July 28, 2010
Revised: September 24, 2010
Published online: January 19, 2011

[1] K. S. Novoselov, A. K. Geim, S. V. Morozov, D. Jiang, Y. Zhang, S. V. Dubonos, I. V. Grigorieva, A. A. Firsov, *Science* **2004**, *306*, 666.
[2] Q. Su, S. P. Pang, V. Alijani, C. Li, X. L. Feng, K. Muellen, *Adv. Mater.* **2009**, *21*, 3191.
[3] A. K. Geim, K. S. Novoselov, *Nat. Mater.* **2007**, *6*, 183.
[4] D. Li, M. B. Mueller, S. Gilje, R. B. kaner, G. G. Wallace, *Nat. Nanotechnol.* **2008**, *3*, 101.
[5] K. S. Novoselov, A. K. Geim, S. V. Morozov, D. Jiang, M. I. Katsnelson, I. V. Grigorieva, S. V. Dubonos, A. A. Firsov, *Nature* **2005**, *438*, 197.
[6] K. S. Novoselov, Z. Jiang, Y. Zhang, S. V. Morozov, H. L. Stormer, U. Zeitler, J. C. Maan, G. S. Boebinger, P. Kim, A. K. Geim, *Science* **2007**, *315*, 1379.
[7] S. Stankovich, D. A. Dikin, G. H. B. Dommett, K. M. Kohlhaas, E. J. Zimney, E. A. Stach, R. D. Piner, S. T. Nguyen, R. S. Ruoff, *Nature* **2006**, *442*, 282.
[8] S. Gilje, H. Song, M. Wang, K. L. Wang, R. B. Kaner, *Nano Lett.* **2007**, *7*, 3394.
[9] P. Blake, P. D. Brimicombe, R. R. Nair, T. J. Booth, D. Jiang, F. Schedin, L. A. Ponomarenko, S. V. Morozov, H. F. Gleeson, E. W. Hill, A. K. Geim, K. S. Novoselov, *Nano Lett.* **2008**, *8*, 1704.
[10] X. Wang, L. Zhi, K. Mullen, *Nano Lett.* **2008**, *8*, 323.
[11] F. Schedin, A. K. Geim, S. V. Morozov, E. W. Hill, P. Blake, M. I. Katsnelson, K. S. Novoselov, *Nat. Mater.* **2007**, *6*, 652.
[12] C. S. Shan, H. F. Yang, J. F. Song, D. X. Han, A. Ivaska, L. Niu, *Anal. Chem.* **2009**, *81*, 2378.
[13] Y. X. Xu, H. Bai, G. W. Lu, C. Li, G. Q. Shi, *J. Am. Chem. Soc.* **2008**, *130*, 5856.
[14] R. S. Sundaram, C. Gomez-Navarro, K. Balasubramanian, M. Burghard, K. Kern, *Adv. Mater.* **2008**, *20*, 3050.
[15] J. Lu, I. Do, L. T. Drzal, R. M. Worden, I. Lee, *ACS Nano* **2008**, *2*, 1825.
[16] G. Goncalves, P. A. A. P. Marques, C. M. Granadeiro, H. I. S. Nogueira, M. K. Singh, J. Gracio, *Chem. Mater.* **2009**, *21*, 4796.
[17] D. H. Wang, D. W. Choi, J. Li, Z. G. Yang, Z. M. Nie, R. Kou, D. H. Hu, C. M. Wang, L. V. Saraf, J. G. Zhang, I. A. Aksay, J. Liu, *ACS Nano* **2009**, *3*, 907.
[18] A. N. Cao, Z. Liu, S. S. Chu, M. H. Wu, Z. M. Ye, Z. W. Cai, Y. L. Chang, S. F. Wang, Q. H. Gong, Y. F. Liu, *Adv. Mater.* **2010**, *22*, 103.
[19] C. Nethravathi, T. Nisha, N. Ravishankar, C. Shivakumara, M. Rajamathi, *Carbon* **2009**, *47*, 2054.
[20] X. M. Geng, L. Niu, Z. Y. Xing, R. S. Song, G. T. Liu, M. T. Sun, G. S. Cheng, H. J. Zhong, Z. H. Liu, Z. J. Zhang, L. F. Sun, H. X. Xu, L. Lu, L. W. Liu, *Adv. Mater.* **2010**, *22*, 638.
[21] Y. Wang, J. Lu, L. H. Tang, H. X. Chang, J. H. Li, *Anal. Chem.* **2009**, *81*, 9710.
[22] X. Liu, H. X. Ju, *Anal. Chem.* **2008**, *80*, 5377.
[23] Z. F. Ding, B. M. Quinn, S. K. Haram, L. E. Pell, B. A. Korgel, A. J. Bard, *Science* **2002**, *296*, 1293.
[24] H. Jiang, H. X. Ju, *Anal. Chem.* **2007**, *79*, 6690.
[25] Y. Shan, J. J. Xu, H. Y. Chen, *Chem. Commun.* **2009**, 905.
[26] G. F. Jie, J. J. Zhang, D. C. Wang, C. Cheng, H. Y. Chen, J. J. Zhu, *Anal. Chem.* **2008**, *80*, 4033.
[27] S. N. Ding, J. J. Xu, H. Y. Chen, *Chem. Commun.* **2006**, 3631.
[28] Y. M. Li, L. H. Tang, J. H. Li, *Electrochem. Commun.* **2009**, 846.
[29] S. Alwarappan, A. Erdem, C. Liu, C. Z. Li, *J. Phys. Chem. C* **2009**, *113*, 8853.
[30] F. R. F. Fan, S. J. Park, Y. W. Zhu, R. S. Ruoff, A. J. Bard, *J. Am. Chem. Soc.* **2009**, *131*, 937.
[31] H. J. Li, J. Chen, S. Han, W. X. Niu, X. Q. Liu, G. B. Xu, *Talanta* **2009**, *79*, 165.
[32] Y. Hernandez, V. Nicolosi, M. Lotya, F. M. Blighe, Z. Y. Sun, S. De, I. T. McGovern, B. Holland, M. Byrne, Y. K. Gun'ko, J. J. Boland, P. Niraj, G. Duesberg, S. Krishnamurthy, R. Goodhue, J. Hutchison, V. Scardaci, A. C. Ferrari, J. N. Coleman, *Nat. Nanotechnol.* **2008**, *3*, 563–568.
[33] G. X. Wang, J. Yang, J. Park, X. L. Gou, B. Wang, H. Liu, J. Yao, *J. Phys. Chem. C* **2008**, *112*, 8192.
[34] J. F. Shen, Y. Z. Hu, M. Shi, X. Lu, C. Qin, C. Li, M. X. Ye, *Chem. Mater.* **2009**, *21*, 3514.
[35] S. Stankovich, R. D. Piner, X. Q. Chen, N. Q. Wu, S. T. Nguyen, R. S. Ruoff, *J. Mater. Chem.* **2006**, *16*, 155.
[36] S. Gilje, S. Han, M. Wang, K. L. Wang, R. B. Kaner, *Nano Lett.* **2007**, *7*, 3394.

[37] N. I. Kovtyukhova, P. J. Ollivier, B. R. Martin, T. E. Mallouk, S. A. Chizhik, E. V. Buzaneva, A. D. Gorchinskiy, *Chem. Mater.* **1999**, *11*, 771.
[38] Y. C. Si, E. T. Samulski, *Nano Lett.* **2008**, *8*, 1679.
[39] G. I. Titelman, V. Gelman, S. Bron, R. L. Khalfin, Y. Cohen, H. Bianco-Peled, *Carbon* **2005**, *43*, 641.
[40] H. L. Guo, X. F. Wang, Q. Y. Qian, F. B. Wang, X. H. Xia, *ACS Nano* **2009**, *3*, 2653.
[41] Z. H. Liu, X. J. Yang, Y. Makita, K. Ooi, *Chem. Mater.* **2002**, *14*, 4800.
[42] Z. T. Luo, Y. Lu, L. A. Somers, A. T. C. Johnson, *J. Am. Chem. Soc.* **2009**, *131*, 898.
[43] Y. Y. Zheng, Z. C. Yang, J. Y. Ying, *Adv. Mater.* **2007**, *19*, 1475.
[44] G. F. Jie, B. Liu, H. C. Pan, J. J. Zhu, H. Y. Chen, *Anal. Chem.* **2007**, *79*, 5574–5581.
[45] G. F. Jie, L. L. Li, C. Chen, J. Xuan, J. J. Zhu, *Biosens. Bioelectron.* **2009**, *24*, 3352.
[46] W. W. Yu, L. H. Qu, W. Z. Guo, Peng, *Chem. Mater.* **2003**, *15*, 2854.
[47] M. Grzelczak, M. A. Correa-Duarte, V. Salgueirino-Maceira, M. Giersig, R. Diaz, L. M. Liz-Marzan, *Adv. Mater.* **2006**, *18*, 415.
[48] B. F. Pan, D. X. Cui, C. S. Ozkan, M. Ozkan, P. Xu, T. Huang, F. T. Liu, H. Chen, Q. Li, R. He, F. Gao, *J. Phys. Chem. C* **2008**, *112*, 939.
[49] Q. W. Li, B. Q. Sun, I. A. Kinloch, D. Zhi, H. Sirringhaus, A. H. Windle, *Chem. Mater.* **2006**, *18*, 164.
[50] J. Lu, I. Do, L. T. Drzal, R. M. Worden, I. Lee, *ACS Nano* **2008**, *9*, 1825.
[51] R. J. Cui, H. C. Pan, J. J. Zhu, H. Y. Chen, *Anal. Chem.* **2007**, *79*, 8494.
[52] X. H. Li, L. Dai, Y. Liu, X. J. Chen, W. Yan, L. P. Jiang, J. J. Zhu, *Adv. Funct. Mater.* **2009**, *19*, 3120.
[53] A. Ramanavicius, A. Finkelsteinas, H. Cesiulis, A. Ramanaviciene, *Bioelectrochemistry* **2010**, *79*, 11.
[54] X. J. Chen, Y. Y. Wang, J. J. Zhou, Y. Wei, X. H. Li, J. J. Zhu, *Anal. Chem.* **2008**, *80*, 2133.
[55] W. S. Hummers, R. E. Offeman, *J. Am. Chem. Soc.* **1958**, *80*, 1339.
[56] K. P. Liu, J. J. Zhang, G. H. Yang, C. M. Wang, J. J. Zhu, *Electrochem. Commun.* **2010**, *12*, 402.
[57] M. H. Yang, Y. Kostov, H. A. Bruck, A. Rasooly, *Anal. Chem.* **2008**, *80*, 8532.